Journal of Structural Geology, Vol. 4, No. 2, pp. 215 to 229, 1982
Printed in Great Britain

0191-8141/82/020215-14 $03.00/0

The effect of material properties on growth rates of folding and boudinage: experiments with wax models

C. NEURATH and R. B. SMITH

Department of Geology and Geophysics, Yale University, New Haven, CT 06520, U.S.A.

(*Received* 21 *May* 1981; *accepted in revised form* 22 *February* 1982)

Abstract—The growth of unstable structures was studied experimentally in layered wax models. The rheological properties of the two wax types were determined independently by a series of cylinder compression tests. Both waxes enhibited (1) a non-Newtonian stress vs strain-rate relationship (2) strain softening and (3) temperature-dependent viscosity. The stress–strain-rate relationships approximated a power-law, with stress exponents of 5 for the microcrystalline wax and 1.8 for paraffin wax.

Blocks of paraffin with a single embedded layer of microcrystalline wax were deformed in two-dimensional pure shear with the layer oriented either parallel to the compressive strain axis so that it shortened and folded, or perpendicular to that axis so that it would stretch and boundinage would form. The growth rates of tiny initial disturbances were measured. The growth rates for folding and boudinage were much higher than could be accounted for by theories assuming Newtonian material properties. Theories taking non-Newtonian behaviour into account (Smith, R. B. 1975. *Bull. geol. Soc. Am.* **86**, 1601–1609; Fletcher, R. C. 1974. *Am. J. Sci.* **274**, 1029–1043) better describe the folding growth rates. Boudinage, however, grew almost three times faster than would be predicted even by existing non-Newtonian theory. A possible reason for this discrepancy is that the waxes do not exhibit steady-state creep as assumed in the theory. We, therefore, extend the theory to include strain-softening. The crucial step in this theory is the use of a scalar measure of the deformation as a state variable in the constitutive law. In this way the isotropic manifestation of strain-softening can be taken into account. The analysis shows that strain-softening can lead to greatly increased boudinage growth rates while having little influence on the growth rates of folds, which is in agreement with the experiments.

INTRODUCTION

THE PURPOSE of this paper is to investigate, experimentally, the influence of material properties on the growth of unstable structures in layered materials. In particular, we will examine the formation of folds and boudinage, both common in the geologic record. Theoretical studies, numerical simulation and previous experimental work have shown that the growth of these structures depends on the contrast in material properties between layers and on the form of the consecutive equation for each layer.

Theoretical analyses of the earliest stages of single-layer folding in Newtonian fluids have been carried out by Biot (1961, 1965), Ramberg (1960), Smith (1975) and Fletcher (1974). This type of analysis has been extended to include non-Newtonian materials, but without memory, by Fletcher (1974) and Smith (1977). The formation of boudinage, in both Newtonian and non-Newtonian materials, has been shown by Smith (1975, 1977) to occur by an instability mechanism which is almost identical to folding. These theories make a direct prediction of how the growth rates of folds and boudinage depend on the constitutive relation for each material. Other more specialized theoretical models have been constructed to demonstrate the effect of non-Newtonian behaviour on the later stages of fold development: Chapple (1968) and DeCaprariis (1974).

A number of authors have attempted to construct numerical models of fold development using the finite element technique (Dieterich & Carter 1969, Parrish 1973, Parrish *et al.* 1976, Shimamoto & Hara 1976). In principle, this method is especially promising as it can include a wide variety of material properties and can follow the growth of the fold to finite amplitude. The existing solutions of this sort are somewhat less useful however, because they have not been closely compared with the fold initiation theories (see above) and because of fundamental questions concerning the modelling of pressure and compressibility.

The generation of folds and boudins has also been studied in the laboratory (Ramberg 1960, Biot *et al.* 1961, Agostino 1971, Hudleston 1973, Cobbold 1975). Only a few researchers have attempted quantitative studies using materials whose stress–strain and stress–strain-rate properties were well known. Hudleston (1973) produced folds in solutions of ethyl cellulose. Unfortunately, there remain questions concerning the true viscosity ratios and the assumption that his materials were in a Newtonian concentration range. The experiments of Biot *et al.* (1961) used Newtonian materials whose properties were adequately documented, but only folding at very high viscosity contrasts (greater than 2000) was investigated. They obtained wavelengths in agreement with their theoretically predicted 'dominant wavelengths'. Only one laboratory study has used carefully characterized non-Newtonian materials. Cobbold (1975) grew folds in paraffin waxes from several initial layer shapes. These experiments cannot be directly compared to the above mentioned theo-

retical models, because the initial layer perturbations were not sinusoidal.

The present experiments were undertaken in an attempt to check more rigorously the existing theories of fold and boudinage initiation and growth. We felt the use of non-Newtonian materials was especially likely to yield new insights, which would allow improved interpretation of natural examples of these two structures.

METHODS

The experimental work was carried out in two parts. First, stress–strain curves were obtained by squeezing wax cylinders at a variety of strain rates and temperatures. From these curves, viscosities and power law exponents were calculated. In the second part of the study, blocks of wax containing single embedded layers were deformed in two-dimensional pure shear to produce folds or boudins. The shear apparatus employed Plexiglas walls so that photographs could be taken during deformation. Rheological parameters determined in cylinder tests were used to interpret the results of model experiments. A brief description of experimental methods follows. Details can be found in the appendix.

Cylinder compression tests

Properties of two waxes, microcrystalline wax (Bennett 1963, Barry & Grace 1971), were determined with an Instron materials testing machine. Moulded test cylinders 4 cm in diameter × 4 cm high, were flattened at constant speed. A continuous record of force was achieved through a calibrated load cell system accurate to ± 1% of full scale. Several deformation rates ranging from 10^{-6} to 10^{-2} s^{-1} were used. Cylinders were maintained at 30, 35 or 40 ± 0.1°C by a water bath. Cylinder ends were lubricated. In converting measured forces to stresses, the calculation was made assuming a homogeneous increase in cross-sectional area.

Special runs were conducted to check the effects of cylinder height-to-diameter ratio, confining pressure, interrupted testing and homogeneity of deformation. The last involved constraining cylinders to deform cylindrically by enclosing them in special telescoping metal sleeves. In total, 39 cylinders were deformed.

Experimental folding and boudinage

Square models 7.5 × 7.5 × 2.5 cm were made by sandwiching a layer of microcrystalline wax between two blocks of paraffin wax. An initial waviness was imparted to the layer by warming and softening the layer and then squeezing it between the hard paraffin blocks on which periodic wavy surfaces had already been machined. The initial amplitude averaged 0.1 times the layer thickness (4 degrees limb dip) for fold-type models and 0.05 times the layer thickness for boudinage-type. Although an attempt was made to give all models equal disturbance amplitudes, some deviated by as much as 35% as shown in the results section. Wavelength for the disturbance was chosen close to the theoretical dominant wavelength. To monitor homogeneity of overall deformation, a square grid was inked onto the surface of the blocks.

A special 'squeeze box' was used within the Instron machine to deform the blocks in two-dimensional pure shear at constant speeds and under confining pressures of about 1 bar. Five features of this apparatus helped achieve these conditions (see Fig. 1).

(1) Top and bottom rams used the motion of the Instron crossheads to squeeze the wax block.

(2) Telescoping L-shaped sidewalls maintained the wax in a rectangular shape.

(3) Rubber top and bottom sheets were glued to the sidewalls. Their stretching motion followed the spreading motion of the deforming block and helped eliminate shear friction between rams and wax.

(4) Rubber air bags connected to a regulated supply of pressurized air maintained constant confining pressure during the entire course of deformation.

(5) Two Plexiglas walls of thickness 2 cm; placed 2.5 cm apart, constrained the deformation to two dimensions and allowed observations and photographs.

The entire apparatus was immersed in a water bath, just as in the cylinder runs, to maintain constant temperature. Silicone grease lubricated all surfaces. Sequential photographs of the deforming block gave sufficient resolution to measure amplitudes of folds and boudins to about ± 0.025 mm which is less than 1% of layer thickness.

RESULTS

Cylinder compression tests

Stress–strain curves at several strain rates are shown for both waxes in Fig. 2. The uniaxial stress (σ) is computed by dividing the measured force by the instantaneous value of the cross-sectional area of the cylinder. (The actual deviatoric stress is 2/3 σ in this geometry). The universal strain rate (ε) is computed by dividing the ram speed by the instantaneous cylinder height. During a single test the strain rate was changed twice or three times to obtain the maximum amount of information (i.e. the so-called interrupted test). Notice that each cylinder underwent a different time history of deformation because different strain-rates were applied in different orders. Yet the stress at any given strain and strain-rate seems quite reproducible.

Paraffin-wax cylinders deformed fairly homogeneously even after natural strains as high as 0.4. In contrast, microcrystalline wax cylinders often developed fractures and/or faults after about 0.2 natural strain. Small fractures formed in a roughly radial pattern. Faults usually occurred on planes at about 45 degrees to the applied stress. In most cases, faults or shear zones eventually gave an hourglass shape to the deformed microcrystalline wax cylinders.

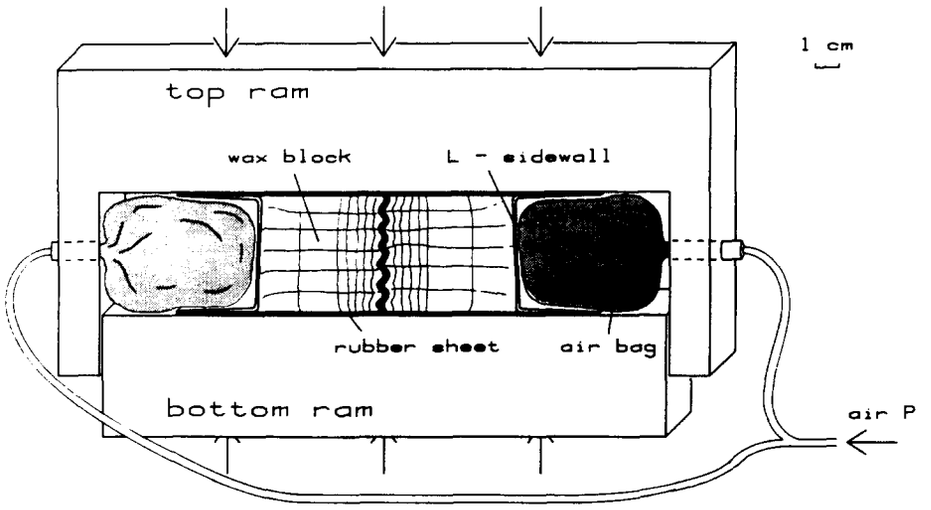

Fig. 1. A cutaway view of the squeeze box for model deformations. Plexiglas front and back walls and their supporting frame are not shown. Rams are machined from aluminum. Telescoping L-shaped sidewalls are made from sheet steel. Thin strips of rubber were glued to the top and bottom pairs of sidewalls. As the sidewalls moved apart the rubber strip would stretch and help produce a homogeneous deformation in the block.

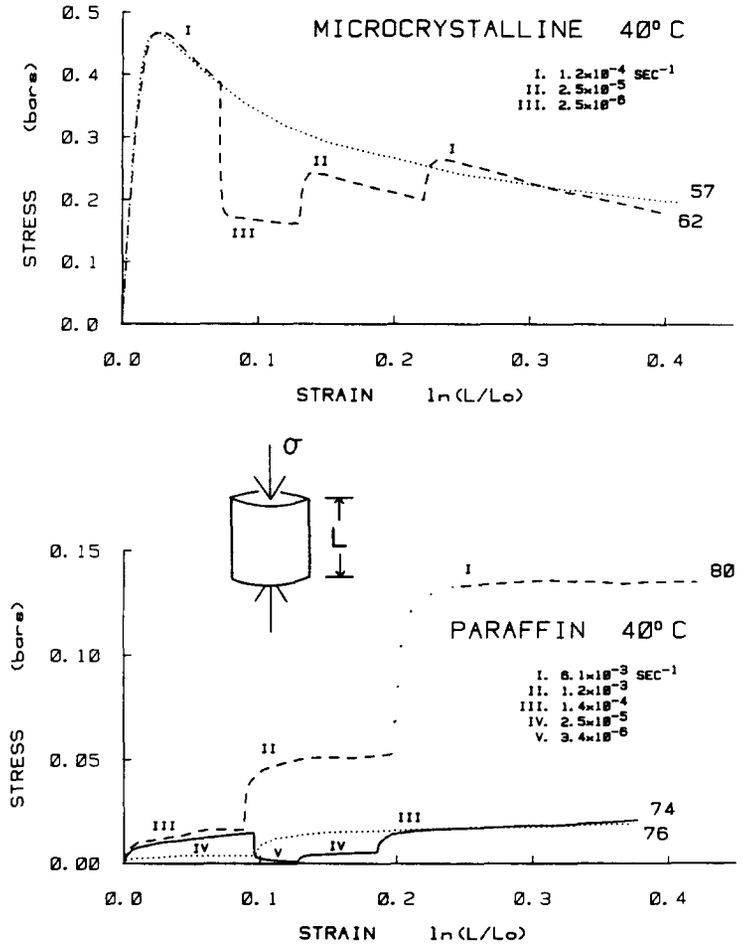

Fig. 2. Stress–strain curves for interrupted uniaxial compression tests on wax cylinders (1 bar = 10^5 Pascals). Roman numerals indicate nominal strain stress rates at different test stages. Notice that paraffin wax is generally much weaker than microcrystalline wax at 40°C but is more sensitive to the strain rate. The dotted portion of run 80 indicates lost data.

The large fractures and faults which are evident in some of the cylinders, do not seem to appear in the later layered experiments. The layered experiments were always performed under confining pressure and were constrained on all sides, as opposed to the cylinders which were usually unconfined. Consequently, the validity of applying rheological parameters derived from cylinder tests to the behaviour of models in a totally different apparatus can be questioned. Obviously the best remedy would be to run stress–strain tests on solid wax blocks in the 'squeeze box' apparatus. Unfortunately, friction forces in the apparatus increased the apparent stress in the deforming waxes so useful data were unobtainable.

However, two justifications do exist for using cylinder tests to interpret layered model experiments. First, fractures and faults were observed only during the latter half of cylinder deformations. Since viscosities were computed from the stress at a strain of 0.1, our conclusions about material properties should hold for the important early stages of the experiments. Second, we were able to do a few special cylinder tests under confining pressure in which the cylinder was constrained to deform cylindrically: conditions which simulate those found in the squeeze box. In these special runs, the incidence of fracturing and faulting was reduced. At the same time, for given strain rates the early stress levels were not changed significantly from those in regular cylinder tests. Although the experiments and data from these special tests are crude, they do provide evidence that confining pressures of the order of 1 bar (1 bar = 10^5 pascals) and certain boundary shape constraints do not greatly alter the waxes' measured viscosities.

Figure 2 shows that at 40°C paraffin wax deforms in nearly steady-state creep while microcrystalline wax is strongly strain softened. As mentioned above, large-scale inhomogeneities may contribute to the strain-softening (weakening) of the microcrystalline wax, but the special runs show that even when inhomogeneities are eliminated by confining pressure and boundary constraints, microcrystalline wax will still exhibit some strain-softening. Perhaps about half as much as appears in these plots.

The other important behaviour shown by these curves is the variation of stress with strain-rate. Stress levels do not change greatly even with large changes in strain-rate for microcrystalline wax, an indication that this wax is non-Newtonian. Paraffin wax is non-Newtonian to a lesser degree. To quantify this behaviour, the data were plotted as log σ against log $\dot{e}$ where σ is stress and $\dot{\epsilon}$ is strain-rate parallel to compression (see Fig. 3). The straight lines on this plot indicate that the waxes obey a power law relationship, $\dot{\epsilon} = C\sigma^N$ with n equal to the inverse of the slope on the plot and C a constant. For microcrystalline wax the exponent n is 5.0, for paraffin wax 1.8.

The viscosity of a deforming material is a measure of its resistance to deformation strain-rate. In the cylinder geometry, the viscosity is computed from the formula $\mu = \frac{1}{3}(\sigma/\dot{\epsilon})$ (Units: pascals s = kg m^{-1} s^{-0} = 10 Poise). In our non-Newtonian materials the viscosity decreases with

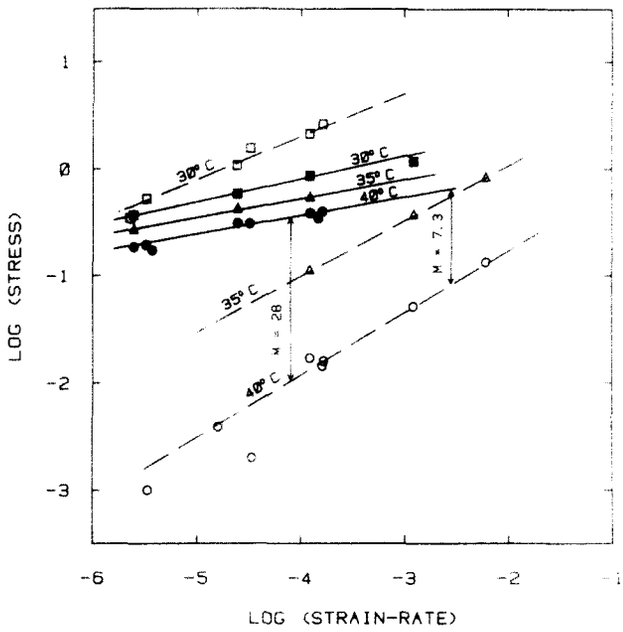

Fig. 3. Master plot showing relationship between strain-rate (s^{-1}) and stress (bars) in wax cylinders at three temperatures. Solid lines and symbols are of microcrystalline wax. Dashed lines with open symbols are for paraffin wax. Since the stress levels varied with strain, stress values shown here were arbitrarily picked off at a strain of 0.1. Lines have an inverse slope equal to the power law exponent. The viscosity contrast, m, between microcrystalline wax and paraffin wax is shown for the conditions which layered models were deformed.

increasing strain-rate. At 40°C the viscosity of paraffin wax ranged from 4×10^6 Pa s^{-1} at low strain-rates to 1×10^6 at high strain rates. Microcrystalline wax went from 2×10^8 to 8×10^6 Pa s^{-1}.

Figure 3 also illustrates the rapid decrease of viscosity with increasing temperature for paraffin wax. The viscosity of microcrystalline wax showed a less dramatic temperature dependence. By choosing appropriate temperatures and strain-rates, we could get a wide range of viscosity contrasts between layer and matrix. At low temperatures or high strain-rate it was even possible to switch over so that paraffin wax was stiffer than microcrystalline wax. Table 1 shows the sets of conditions at which we chose to run model deformation experiments. Paraffin wax was chosen as the matrix because it was generally softer than microcrystalline wax and because it resisted faulting initiated at the boundaries of the squeeze box.

Experimental folding and boudinage

Four cases were covered by the model experiments: folding with viscosity contrasts of 7.3 and 28 and boudinage with viscosity contrasts of 7.3 and 28. Two

Table 1. Deformation conditions and rheological parameters in model experiments

Temperature (°C)	Strain rate ($\times 10^{-4}$ s^{-1})	Viscosity ratio	Paraffin power law exponent	Microcrystalline power law exponent
40	0.29	7.3	1.8	5.0
40	1.1	28	1.8	5.0

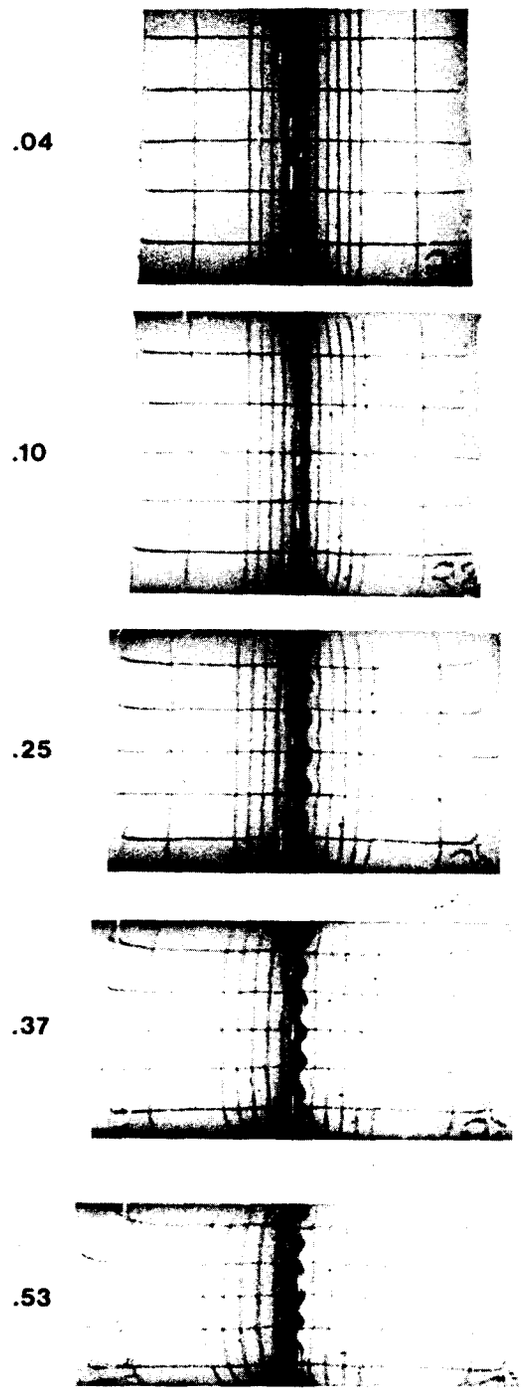

Fig. 4. Photographs show progressive stages of deformation in the squeeze box. Over all strain (In L/L_0) is given by numbers to left of pictures. (a) Folding at viscosity contrast of 28, block No. 38, white spots are reflections.

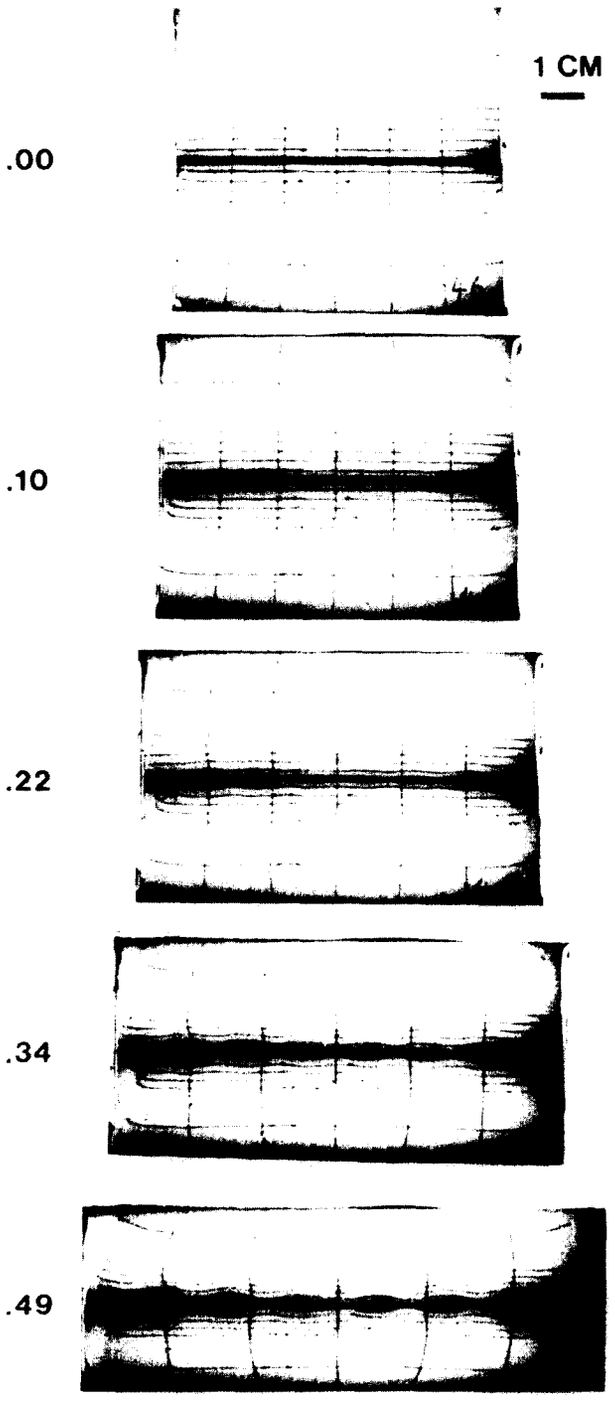

Fig. 4(b) Boudinage at viscosity contrast of 7.3, block No. 46

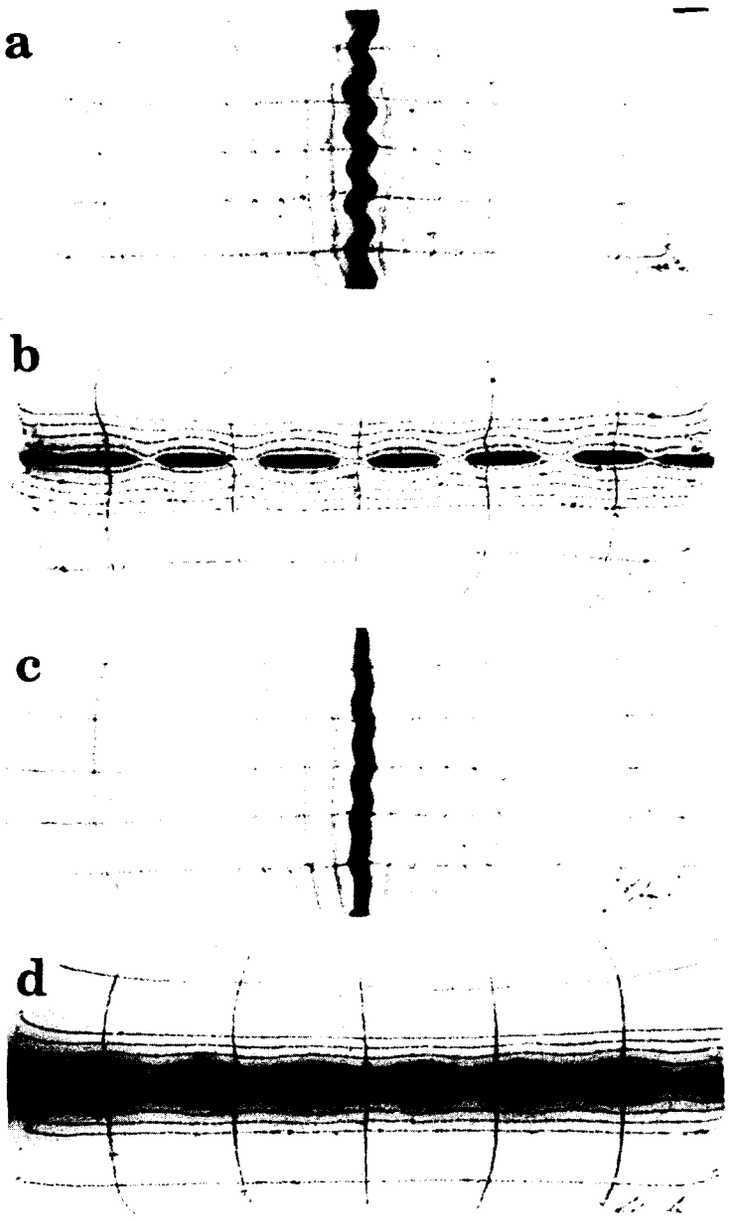

Fig. 5. Final photographs of model blocks after a total natural strain of 0.5, showing layer structures and passive grid lines in the four experimental cases. (a) Folding at viscosity contrast, m, of 28, block No. 38, (b) boudinage at $m = 28$, block No. 45, (c) folding at $m = 7.3$, block No. 41, (d) boudinage at $m = 7.3$, block No. 46. Note that the folded layers (a) and (c) show a light edge. This is a thin rim of translucent wax which flared out against the Plexiglas walls. The actual layer is about 20% thinner than these final pictures of the block surface seem to show.

runs were made for each case to check reproducibility. Regular trains of folds or boudins grew in all experiments. Figure 4 shows progressive stages of deformation during folding and boudinage experiments. Also illustrated by the photographs is the capability of the apparatus for giving a fairly homogeneous overall deformation, even at the largest strains. Strains measured at the grid lines about one wavelength from the layer were within 5% of strains indicated by the boundary displacements. The layer remained well bonded to the matrix throughout the deformations, with little apparent slip or separation.

Fold and boudin shapes were not studied systematically. It was noted, however, that the folds started as similar folds and spot measurements showed a thickening in the hinges and thinning in the limbs after large deformations.

Large-amplitude boudins, especially those grown with a viscosity contrast of 28, also deviated from the sinusoidal shape assumed in Smith's (1975, 1977) theory. The pinches accentuated into cusps, which eventually produced fairly sharp separations between the boudins. Then the lozenge-shaped boudins pulled away from each other and ceased flattening (see Fig. 5b). Another deviation from sinusoidal shape probably occurred because the layer thickness was progressively reduced, thereby shortening the dominant wavelength. Consequently, some of the stretched swells developed secondary boudinage pinches in their middles. In similar fashion, the thin drawn-out sections of the pinches developed secondary very short wavelength boudinage. Examples of secondary boudinage are rarely visible in Fig. 5d in both pinch and swell areas of the centre primary boudin.

The most useful parameters derived from the deformation experiments were growth rates. The normalized growth rate, γ, is defined here based on Smith (1977) as $dA/A = \gamma dL/L$ where A is the disturbance amplitude and L is the length of a passive marker line far from and parallel to the layer. After integration: $\ln A/A_0 = \gamma \ln L/L_0$. Therefore, to determine γ we plotted in $\ln A/A_0$ (normalized amplitude) against $\ln L/L_0$ (natural strain parallel to layer) in Fig. 6. The slope of this curve at any point equals the growth rate. To keep within a linear regime of small amplitude homogeneous deformation, the growth rate was determined from the first few points at strains less than 0.2. Fitting was by least mean squares. Growth rates are tabulated in Table 2 along with the conditions under which models were deformed. The lack of complete reproducibility is probably due to inconsistencies in wax molding or layer emplacement.

One should note from Fig. 6 that growth does not continue increasing at the initial rate but levels off, presumably because after a certain amplitude is reached, the growth mechanism changes. The absolute amplitude achieved at the onset of nonlinear growth, ranges between 20 and 30 degrees limb dip for folding and 7 and 20 degrees dip for boudinage.

DISCUSSION

Reasons for studying growth rates

Contrary to most previous work, this study has focused on growth rates rather than wavelengths. There are several reasons for this choice.

First, one can bypass the requirement of knowing the relationship between initial layer irregularities and final wavelength. Fletcher & Sherwin (1978) point out that in the special case where the initial surface contains a 'white roughness' spectrum of wavelengths of equal

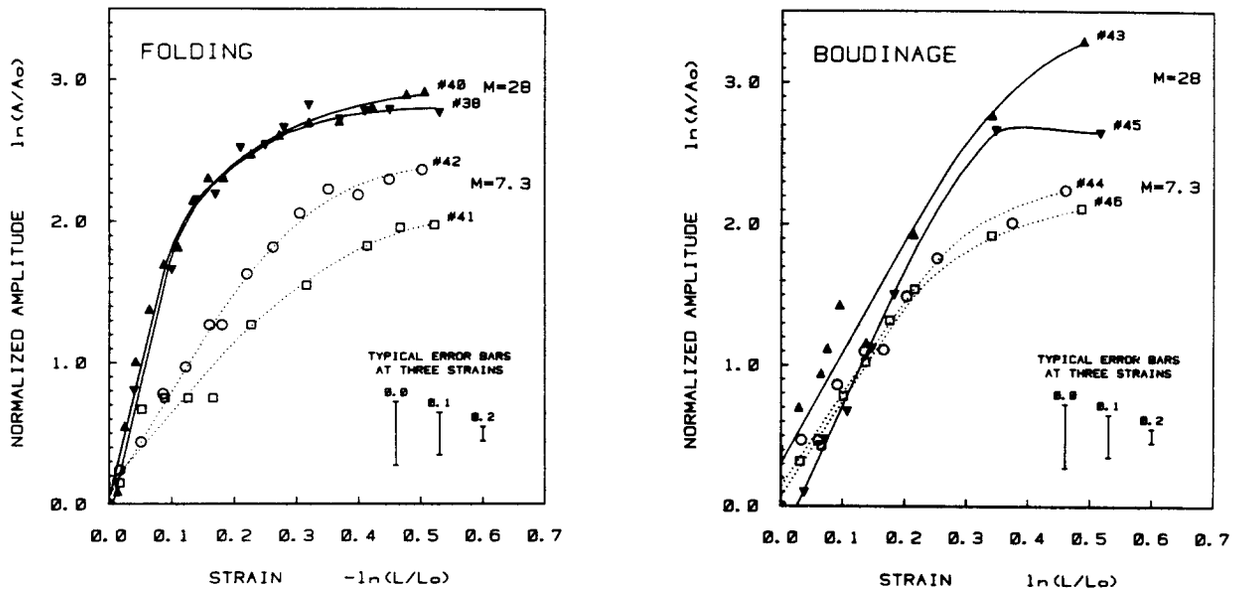

Fig. 6. The amplitude of folding and boudinage plotted against overall strain. Each amplitude point is the average for six individual folds or boudins developed in a layer. Error bars correspond to the standard deviation of ten repeated measurements on a single typical fold or boudin. Solid symbols are experiments at conditions giving m = 28; open symbols are experiments at m = 7.3. The growth rate is computed from the slope of the linear part of the curve.

Table 2. Growth rates of experimental folding and boudinage

Model No.	Initial amplitude (a_0/H)	Wavelength to thickness ratio* (λ/H)	Viscosity contrast* (m)	Observed growth rate† (γ)	Theoretical growth rates: Newtonian $n_1=1, n_2=1$ (γ)	Non-Newtonian $n_1=1.8, n_2=5.0$ (γ)	Non-Newtonian and strain-softening‡ (γ)
Folding:							
38	0.092	8	28	18.0 ± 0.7 (3 points)	9.4	19.7	21($n_{eff}=7$)
40	0.092	8	28	18.0 ± 0.4 (7 points)	9.4	19.7	21($n_{eff}=7$)
41	0.087	8	7.3	4.8 ± 0.7 (7 points)	3.8	6.5	7($n_{eff}=100$)
42	0.076	8	7.3	7.1 ± 0.3 (8 points)	3.8	6.5	7($n_{eff}=100$)
Boudinage:							
43	0.031	6	28	8.6 ± 2.3 (6 points)	−0.1	3.3	9($n_{eff}=15$)
45	Data missing	6	28	8.5 ± 0.7 (6 points)	−0.1	3.3	9($n_{eff}=15$)
44	0.044	6	7.3	6.7 ± 0.6 (7 points)	−0.3	1.6	4($n_{eff}=28$)
46	0.063	6	7.3	7.3 ± 0.1 (6 points)	−0.3	1.6	4 ($n_{eff}=28$)

* Nominal values determined at a strain of 0.1.
† These slopes are calculated from the initial linear portion of the curves in Fig. 3 and are given with the standard error of slope. The number of points from which the slope was determined is given in parentheses. The overall uncertainty in the growth rates is much larger than the indicated values, as is evident from the lack of reproducibility, for example between model numbers 41 and 42.
‡ Approximate values due to uncertainty in estimating degree of strain-softening in waxes.

limb dips, the periodic wave train which eventually develops will in fact have an average wavelength equal to the theoretical dominant wavelength. In laboratory experiments, however, 'white roughness' is difficult to impress into a layer. Also, to get a statistically valid wavelength, large numbers of waves must be grown. Williams *et al.* (1978) have concluded from experimental and computer simulation studies that the relationship between initial and final shape of layers is complex.

In contrast, the normalized growth rate of disturbance is theoretically independent of the initial amplitude as long as the amplitude is small. Shimamoto & Hara's (1976, fig. 3c) results with computer finite-element folding, support this hypothesis. Initial limb dips were set at 1, 4 or 10 degrees yet folds grew at equal rates. In our experiments, consistent results were most easily obtained by measuring growth rates of regular structures which had been induced by an initial periodic layer waviness.

Another reason for concentrating on growth rates is because they exhibit a much greater variation with changing material rheology than do dominant wavelengths. Growth rates are, therefore, more characteristic of a particular rheological combination. Over the range of conditions with which we worked, the theory predicts that dominant wavelengths should vary only by ± 20% while the growth rates should vary by ± 250% for folding and by ± 300% for boudinage. These relationships are shown by Smith (1977, figs. 6, 7 and 8).

All the above reasons for working with growth rates come from the fact that the amplitude of a growing disturbance is simply a more direct measure of the growth mechanism than is wavelength. When one measures an observed final wavelength, one is choosing an integrated parameter incorporating the growth rates of many wavelengths. A more precise and easily defined measure is the growth rate of a single wavelength.

The disadvantage of focusing on growth rates arises during attempts to relate them directly to structures observed in rocks. Often little or no time history exists in an outcrop from which to determine growth rates. Wavelengths, on the other hand, can be easily measured in the field.

Theoretical versus observed growth rates

The growth rates observed in our experiments can be compared with those predicted by theory. As shown in Table 2, the experimental growth rates for folding were close to those expected from Smith's (1977) non-Newtonian theory. Boudinage, however, grew much faster than would be predicted.

Why should fold growth rates be so close to those predicted and boudinage growth rates so far off? Before trying to answer this question we will re-examine the experimental conditions and see how closely they fit the assumptions on which the theory is based.

I. *Material properties.*

(a) *Are the waxes homogeneous and isotropic*? Slight inhomogeneities existed due to the moulding process, such as small air bubbles, but otherwise the waxes' appearance and behaviour led us to believe they are homogeneous and isotropic.

(b) *Did waxes exhibit steady-state creep*? No, after a few per cent strain, the microcrystalline wax was strongly strain-softened. During later stages of deformation, shears and fractures became visible. Paraffin wax strain-softened at low temperatures but at 40°C exhibited approximately steady-state creep.

II. *Deformation conditions*

(a) *Did cylinders and models deform in homogeneous*

pure shear? Yes, the passive grid shows good homogeneity throughout the deforming blocks. Only near the boundaries did distortion become extreme, due to friction. So that this distortion would not influence our results, we made all layer measurements at points more than one wavelength away from boundaries.

(b) *Were folding layers parallel to compressive strain and boudinage layers perpendicular to compressive strain*? Yes, within a few degrees.

(c). *Could material parameters determined in uniaxial cylinder tests be applied to 2-D model block experiments*? This problem is discussed above in the results section under Cylinder compression tests. For the following reasons we conclude that rheologies determined in cylinder tests should apply to our model experiments. (1) We were only interested in the quantitative aspects of early growth stages. During these stages cylinders and blocks appeared to behave similarly, that is, no fractures or faults were visible in either. (2) Confining pressure and shape constraints were applied in a few cylinder tests to simulate squeeze box conditions and they did not greatly alter stress–strain curves. (3) Different cylinder geometries were used including tall, thin and short, flat shapes. Again, stress–strain curves were not appreciably affected.

(d) *Is small amplitude theory applicable to our experimental folding and boudinage*? The theory is based on infinitesmal deformations but is assumed to hold for small amplitudes. Chapple (1968) has suggested 5 degree limb dip as the limit of applicability while we obtained linear growth rates up to limb dips of 7 to 30 degrees depending on conditions.

(e) *Were the layers long enough to be considered of infinite length*? Yes, boudinage layers will stretch with the surrounding matrix only if the ratio of layer length to layer height is large in comparison to the viscosity contrast (m) between layer and matrix. For $m = 28$, we had a length/height ratio of 50. From observations, the boudinage layers did strain with the matrix (as seen in Figs. 5b & d) with only a slight lag at each end. The folding layers, being in direct contact with the moving rams, always strained with the matrix.

Of the above conditions, we feel the most likely cause for the discrepancy between observed and theoretical growth rates was I(b), lack of steady-state creep. Finite amplitude effects, II(d), could also play a role, but are difficult to quantify. The following analysis extends earlier theory beyond the assumption of steady-state creep, to include strain-softening materials such as the microcrystalline wax.

The theory of layer instabilities in strain-softening materials

The existing theories of layer instability in non-Newtonian materials take into account only the variation of the viscosity function μ with the rate-of-strain. Yet, in many materials, the resistance to deformation also depends on the total strain which has occurred since the substance was formed from a melt or most recently annealed. The weakening of a material with increasing strain (i.e. strain-softening) could arise, for example, by an increase in the density of dislocations, voids, or microcracks as the deformation proceeds (e.g. White *et al.* 1980).

One important consequence of the strain-softening of the more competent layer is that the viscosity ratio (m) will be decreasing during the experiment. This would tend to progressively decrease the growth rates. A less obvious but equally important effect is that, because of the perturbation strain field associated with (say) folding, different regions in the folding layer will soften at different rates. This effect may add directly to the strain-rate softening effect as it is the higher/lower strain-rate regions which will also have a higher/lower strain. To investigate this effect we need to construct a careful model of fold and boudinage growth in a strain and strain-rate softening material.

In order to represent these properties mathematically we shall attempt to use the Reiner–Rivlin equation (e.g. Smith 1979) in two dimensions, extended to include the scalar strain θ as a state variable.

$$\sigma_{ij} = -p\delta_{ij} + \mu(\theta, \dot{\theta})\dot{\varepsilon}_{ij}. \qquad i, j = 1, 2. \tag{1}$$

The viscosity function μ thus depends on both the scalar strain θ and the scalar rate-of-strain $\dot{\theta}$.

$$\begin{aligned} \theta &= \varepsilon_{11}^2 + 2\varepsilon_{12}^2 + \varepsilon_{22}^2 = \text{trace } \varepsilon_{ik}\varepsilon_{kj} \\ \dot{\theta} &= \dot{\varepsilon}_{11}^2 + 2\dot{\varepsilon}_{12}^2 + \dot{\varepsilon}_{22}^2 = \text{trace } \dot{\varepsilon}_{ik}\dot{\varepsilon}_{kj} \end{aligned} \tag{2}$$

where

$$\dot{\varepsilon}_{ij} = \frac{d}{dt}\varepsilon_{ij}. \tag{3}$$

This constitutive relation describes a material with a memory of its initial state but without elasticity. The deviatoric stress $\sigma_{ij} + p\delta_{ij}$ is zero when $\dot{\varepsilon}_{ij} = 0$. Using the scalar θ as a state variable allows us to represent only 'isotropic' strain softening caused by isotropic changes in the microscopic structure of the material.

In order to investigate the nature of small disturbances on a basic state, we derive a constitutive law that relates perturbation stress, strain and strain rate at each point. To begin, we represent the stress, strain, and strain rate as the sum of a basic value (S, E, $\dot{E}$) and a perturbation (primed variables):

$$\begin{aligned} \sigma_{ij} &= S_{ij} + \sigma'_{ij} \\ \varepsilon_{ij} &= E_{ij} + \varepsilon'_{ij} \\ \dot{\varepsilon}_{ij} &= \dot{E}_{ij} + \dot{\varepsilon}'_{ij}. \end{aligned} \tag{4}$$

Putting these into (1), linearizing and subtracting off the basic state terms gives

$$\sigma'_{ij} = -p'\delta_{ij} + \mu(\bar{\theta}, \bar{\dot{\theta}})\dot{\varepsilon}'_{ij} + \mu_\theta\theta'\dot{E}_{ij} + \mu_{\dot{\theta}}\dot{\theta}'\dot{E}_{ij}, \tag{5}$$

where μ_σ and μ_σ are derivatives evaluated at the basic state conditions $\bar{\theta}$, $\bar{\dot{\theta}}$, which are in turn, functions of time. For the case considered here $\dot{E}_{11} = -\dot{E}_{22}$, $\dot{E}_{12} = 0$, so that the third and fourth terms on the right side of

(5) do not influence the tangential stresses. From (2),

$$\theta' = 2E_{11}\varepsilon'_{11} + 2E_{22}\varepsilon'_{22}$$
$$\dot{\theta}' = 2\dot{E}_{11}\tilde{\varepsilon}'_{11} + 2\dot{E}_{22}\tilde{\varepsilon}'_{22}. \tag{6}$$

Equation (5) now becomes

$$\sigma'_{11} = -p + \mu\left(1 + \frac{\mu_\theta}{\mu}\dot{E}_{11}4E_{11}\frac{\varepsilon'_{11}}{\tilde{\varepsilon}'_{11}} + \frac{\mu_{\dot\theta}}{\mu}\dot{E}_{11}4\dot{E}_{11}\right)\tilde{\varepsilon}_{11}$$
$$\sigma'_{12} = \mu\varepsilon'_{12} \tag{7}$$
$$\sigma'_{22} = -p + \mu\left(1 + \frac{\mu_\theta}{\mu}\dot{E}_{11}4E_{11}\frac{\varepsilon'_{22}}{\tilde{\varepsilon}'_{22}} + \frac{\mu_{\dot\theta}}{\mu}\dot{E}_{11}4\dot{E}_{11}\right)\tilde{\varepsilon}_{22}.$$

For most time-dependent flows there would be no simple relationship between ε_{ij} and $\tilde{\varepsilon}_{ij}$ other than (3). For small amplitude layer instabilities however

$$E_{ij} = \dot{E}_{ij}t. \tag{8}$$

If the perturbation structure is growing exponentially then

$$\tilde{\varepsilon}'_{ij} = f(x, y)e^{\alpha t} \tag{9}$$

and

$$\varepsilon'_{ij} = \frac{f}{\alpha}e^{\alpha t} - \frac{f}{\alpha}. \tag{10}$$

If the initial amplitude of the perturbation structure is very small, then we are interested in the disturbance after considerable growth has occurred ($\alpha t > 1$). In this case

$$\varepsilon'_{ij} \approx \frac{f}{\alpha}e^{\alpha t} = \frac{\tilde{\varepsilon}_{ij}}{\alpha}. \tag{11}$$

To obtain a tractable problem we select a viscosity function of the form

$$\mu(\theta, \dot{\theta}) = \hat{\mu}(\dot{\theta})e^{-(\theta/\theta^*)^2}, \tag{12}$$

where θ^* is a measure of the strain-softening in the material. This single parameter separable function is somewhat restrictive, but it allows us to derive a time independent formula for an 'effective' power law exponent which incorporates the primary effects of strain-softening.

The stress–strain curves from the uniaxial cylinder tests can be used to determine θ^* in the following way. If the uniaxial strain ε, is taken in the direction '1', then

$$\varepsilon = \varepsilon_{11} = -2\varepsilon_{22} = -2\varepsilon_{33} \tag{13}$$

so that

$$\theta = \frac{3}{2}\varepsilon^2. \tag{14}$$

From (1) and (12), the deviatoric stress will drop to (1/e) of its initial value when $\theta = \theta^*$ or, using (14), when $\varepsilon = \varepsilon^*$ given by

$$\theta^* = \frac{3}{2}\varepsilon^{*2}. \tag{15}$$

The value ε^*, which characterizes the degree of strain-softening, can be read from the stress–strain curves. If the stress drop is rapid, ε^* will be small and strain-softening is important.

For use in (7), we now differentiate (12)

$$\frac{\mu_\theta}{\mu}\Big|_{\dot\theta} = -\frac{1}{2}(\bar{\theta}, \theta^*)^{-1/2}. \tag{16}$$

From (15) and (16), with $\dot{\theta} = 2\dot{E}_{11}^2$ we have

$$\frac{\mu_\theta}{\mu}\Big|_{\dot\theta} = \frac{-1}{2\sqrt{3}\,\varepsilon^* E_{11}}. \tag{17}$$

Using (17) the coefficient of $\tilde{\varepsilon}_{11}$ in (7) becomes

$$\eta = \mu(\bar{\theta}, \bar{\dot{\theta}})\left(1 - \frac{2}{\sqrt{3}\,\gamma\varepsilon^*} + 2r\right), \tag{18}$$

where 'γ' is the normalized growth rate

$$\gamma \equiv \frac{\alpha}{\dot{E}_{11}} \tag{19}$$

and 'r' is a measure of strain rate softening

$$r \equiv \frac{\bar{\dot\theta}\mu_{\dot\theta}}{\mu}. \tag{20}$$

For a power-law dependence of strain-rate upon stress, the quantity 'r' can be shown to be equal to $[1/2(1/n - 1)]$, where 'n' is the stress-exponent. Finally then using this, and (18)

$$\eta = \mu(\bar{\theta}, \bar{\dot{\theta}})\left(\frac{1}{n} - \frac{2}{\sqrt{3}\,\gamma\varepsilon^*}\right). \tag{21}$$

For instabilities with rapid growth rates, or in materials with little strain-softening (i.e. large ε^*) (21) reduces to

$$\eta = \mu/n$$

as in Smith (1977, 1979). More generally, we can characterize the combined effect of strain and strain-rate softening by defining an effective power law exponent

$$\frac{1}{n_{\text{eff}}} \equiv \frac{1}{n} - \frac{2}{\sqrt{3}\,\gamma\varepsilon^*}. \tag{22}$$

This exponent can be used directly in the formulae for the dynamic growth rate of folds and boudins derived by Smith (1977, 1979) written schematically as

$$\gamma_d = \gamma_d(\gamma/H, m, n_1, n_2). \tag{23}$$

The two formulae, (22) and (23), must be solved simultaneously to determine γ and n_{eff}.

Using (22) we can estimate the role of strain-softening in the present experiments. For the paraffin, the cylinder tests indicate $n = 1.8$ and $\varepsilon^* = 10$ or greater or even negative (i.e. little if any strain-softening, possibly

strain-hardening). Even for the slowest growth observed in the experiments, $\gamma = 6$, equation (22) gives $n_{\text{eff}} \approx n$. For the microcrystalline wax (i.e. the layer material), the cylinder tests indicate $n = 5$, with ε^* being somewhat greater than 0.3 depending on the confining pressure and the way the curve fitting is done. We will use a value of $\varepsilon^* = 1$ in the following estimates.
Then for folding:

$$m = 28, \text{ observed } \gamma \approx 18$$

$$\frac{1}{n_{\text{eff}}} = \frac{1}{5} - \frac{1.15}{18(1)} \approx \frac{1}{7} \tag{24}$$

$$m = 7.3, \text{ observed } \gamma \approx 6$$

$$\frac{1}{n_{\text{eff}}} = \frac{1}{5} - \frac{1.15}{6(1)} \approx \frac{1}{100} \tag{25}$$

and for boudinage:

$$m = 28, \text{ observed } \gamma \approx 8.5$$

$$\frac{1}{n_{\text{eff}}} = \frac{1}{5} - \frac{1.15}{8.5(1)} \approx \frac{1}{15} \tag{26}$$

$$m = 7.3, \text{ observed } \gamma \approx 7$$

$$\frac{1}{n_{\text{eff}}} = \frac{1}{5} - \frac{1.15}{7(1)} \approx \frac{1}{28}. \tag{27}$$

The high contrast folding (24) is not significantly influenced by strain-softening because of its large growth rate. High contrast boudinage (26) is more strongly affected. Low contrast folding and boudinage (25) and (27) are, if we can believe the choice $\varepsilon^* = 1$, very strongly influenced by strain-softening because of their small growth rates.

In these latter cases, very large values of n_{eff} will be generated by the cooperation of strain and strain-rate softening. Because of the large value of n_{eff} the calculation of the growth rates can be simplified using the technique of Smith (1977, 1979) with $n_2 = \infty$. The length of this calculation can be further reduced if we follow the Appendix in Smith (1979) with $n_1 = 1$. The algebra still takes several pages but the result, for boudinage, is

$$\gamma_d = \frac{-(m-1)(2m\tan\beta)}{m + \beta - \tan\beta + (m+\beta)\tan^2\beta} \tag{28}$$

and for folding

$$\gamma_d = \frac{(m-1)(2m\tan\beta)}{m + \beta + \tan\beta + (m+\beta)\tan^2\beta}, \tag{29}$$

where $\beta \equiv \pi H/\lambda$ and $\gamma = \gamma_d + 1$. An equivalent derivation has been done by Fletcher (1981).

These functions have a broad maximum at about $\lambda/H = 4$, and for $m \geq 2$, this maximum growth rate is approximately (from 28, 29)

$$\gamma_d \approx m - 1.3 \text{ for boudinage}$$
$$\gamma_d \approx m - 2.5 \text{ for folding.} \tag{30}$$

The values given by (30) would have to be increased by about 20% to take into account the fact that $n_1 = 1.8$ rather than $n_1 = 1$.

Note that for very large n_{eff} it is no longer appropriate to think of folding as the faster-growing instability. Choosing $m = 7.3$ gives $\gamma_d = 7$, $\gamma \approx \gamma_d - 1 \approx 6$, $\gamma = \gamma_d + 1 \approx 7$, is not much different. This agrees with the observed values ($\gamma \approx 7$ for boudinage, $\gamma \approx 6$ for folding) within the accuracy and repeatability of the experiments. A more direct comparison, using the exact growth rate equations, is presented in Table 2.

The above reasoning is particularly helpful in explaining how boudinage can form in materials with modest viscosity ratios and power law exponents. Without strain-softening, the values $n_2 = 5$, $n_1 = 1.8$, $m = 7.3$ give a growth rate of $\gamma = 1.6$. It is doubtful that boudinage could be generated at all with a growth rate this low.

The reader has probably already noticed that by choosing a smaller value of ε^* in (22), or a larger value of n, it is possible to make n_{eff} negative. The physical meaning of this situation is clarified by the energy analysis of Smith (1981). With n_{eff} negative it is possible for a disturbance to draw energy directly from the basic state strain-energy stored in the material. In a large block of such material, this situation would lead to catastrophic failure, if the boundary conditions would allow it. If, however, a thin layer has a negative value for n_{eff}, its surroundings with positive n_{eff} will act to keep the growth rate of moderate wavelength disturbances bounded. In this case the growth rates of a disturbance could be even larger than in the $n_2 \to \infty$ limit, as given by (28) and (29), as there is now an additional source of energy. The disturbance can draw energy both from the jump in the layer-parallel normal stress across the tilted interfaces (Smith 1975, 1977) and, from the interior of the strain and strain-rate softening layer.

This latter source is one that allows far reaching conjugate shear zones to form in straining homogeneous materials (Smith 1981). Such shear zones were seen to develop around small interior or boundary imperfections in large blocks of the microcrystalline wax during two-dimensional deformation experiments and in the cylinder compression tests described earlier. The theory allows us to see the three observations: strain and strain-rate softening of cylinders, conjugate shear zone formation in large blocks and rapid growth of boudinage in thin layers, as closely related phenomena.

The reader is certainly aware of the speculative nature of this discussion in relation to the wax experiments. The uncertainty in the empirically derived material properties and growth rates, together with assumptions (11) and (12) in the analysis, cloud the results. More careful experiments, together with numerical modelling, may be necessary to determine more quantitively the influence of strain-softening on layer instabilities.

Comparison of experimental results to previous fold modelling studies

To compare previous studies to the present experi-

Table 3. Growth rates of experimental and finite-element folding

Type	Model	n Matrix	n Layer	λ_0/H_0	m	Observed growth rate	Theoretical growth rate
Wax	Cobbold 1	2.6	2.6	?*	10	5.5	7.6*
experiments	Cobbold 2	2.6	2.6	?*	10	8.3	
	Cobbold 3	2.6	2.6	?*	10	7.1	
Finite-element	Shimamoto	1	1	7.4	10	4.0	4.8
	and Hara	1	1	11	30	8.5	11.0
		1	1	16	100	20	25.5
Finite-element	Parrish	5	8	9	12	4.6	17.1
Finite-element	Parrish *et al.*	8.3	2.6	9	10	5(?)†	12.0

*The initial disturbance for the three models were of different shape and amplitude, but none was periodic or sinusoidal so no wavelength is given here. The theoretical growth rate is that for a sinusoidal waveform of "dominant" wavelength/thickness ratio. See text for further explanation.

†Rough estimate due to incomplete published data set.

mental results we computed growth rates from diagrams or graphs available in four published papers. Table 3 lists the parameters for the models and both the observed and theoretical growth rates. The laboratory experiments of Cobbold (1975) used materials whose rheology was carefully determined. Cobbold's initial layer shapes, which were neither sinusoidal nor periodic, had no well-defined wavelength. Nevertheless, his layers tended to develop a periodic sinusoidal shape and a dominant wavelength during growth. This should allow comparison of Cobbold's growth rates with the present results. The other three studies were with finite-element computer models. Shimamoto & Hara (1976) assumed Newtonian rheologies while Parrish (1973) and Parrish *et al.* (1976) had models incorporating power law rheologies.

Looking at these four studies and including ours as a fifth, it seems that the observed growth rates for the first two correspond adequately to the predicted values from theory. The two finite-element studies with power law materials gave growth rates much lower than would be predicted. Our experimental results in strain-softening materials, required an addition to the theory in order to account for the large boudinage growth rates. In conclusion, it is difficult to see any consistent relationships between observed and theoretical growth rates for the five studies. Methodological differences between the studies as well as parameters which have not been taken into account (those besides n_1, n_2, m and λ_0/H_0) probably cause the inconsistent growth rate results.

Experimental rock deformation work

Experimental deformation data from a wide variety of rocks and minerals have generally been fitted to a power law equation with exponents between 2 and 8 (Tullis 1979, Carter 1975). As for evidence of strain-softening in rocks, Griggs *et al.* (1960) give stress–strain curves at 5 kb confining pressure and strains of about 15% for several rock types. Dunite, pyroxenite and Yule marble (see also Heard & Rayleigh 1972) showed either steady-state deformation or strain-hardening. But basalt, granite and dolomite all exhibited strain-softening over a wide range of experimental conditions. Quartzite has also shown some strain-softening in Heard & Carter's (1968) experiments. Paterson & Weiss (1966, 1968) deformed an anisotropic rock, phyllite, by 20% or more and obtained strain-softening when shortening was parallel or at a low angle to the foliation. Their experiments also produced folding and boudinage of quartz veins running through the phyllite.

Experimental results from rock studies support the belief that our waxes' rheologies are appropriate for modelling small fracture formation in some rocks of the Earth's crust. It may be interesting to find out whether folds and boudins (especially the latter) are more often found in rock types exhibiting strain-softening rather than steady-state creep or strain-hardening.

Acknowledgements—We thank Robert B. Gordon for the use of the Instron materials testing machine and associated facilities. The paper has benefited from the constructive criticism of two anonymous reviewers.

REFERENCES

Agostino, P. N. 1971. Theoretical and experimental investigations on ptygmatic structures. *Bull. geol. Soc. Am.* **82**, 2651–2660.

Barry, B. W. & Grace, A. J. 1971. Rheological properties of white soft paraffin. *Rheol. Acta* **10**, 113–120.

Bennet, H. 1963. *Industrial Waxes*, Vol. 2. Chemical Publishing Co., New York.

Biot, M. A. 1961. Theory of folding of stratified viscoelastic media and its implications in tectonics and orogenesis. *Bull. geol. Soc. Am.* **72**, 1595–1620.

Biot, M. A. 1965. *Mechanics of Incremental Deformation*. John Wiley & Sons, New York.

Biot, M. A., Ode, H. & Roever, W. L. 1961. Experimental verification of the theory of folding of stratified viscoelastic media. *Bull. geol. Soc. Am.* **72**, 1621–1632.

Carter, N. L. 1975. High-temperature flow of rocks. *Rev. Geophys. Space Phys.* **13**, 344–349.

Chapple, W. M. 1968. A mathematical theory of finite-amplitude rock-folding. *Bull. geol. Soc. Am.* **79**, 47–68.

Cobbold, P. R. 1975. Fold propagation in single embedded layers. *Tectonophysics* **27**, 333–351.

DeCapraris, P. 1974. Stress-induced viscosity changes and the existence of dominant wavelengths in folds. *Tectonophysics* **23**, 139–148.

Dietrich, J. H. & Carter, N. L. 1969. Stress-history of folding. *Am. J. Sci.* **267**, 129–154.

Fletcher, R. C. 1974. Wavelength selection in the folding of a single layer with power-law rheology. *Am. J. Sci.* **274**, 1029–1043.

Fletcher, R. C. 1981. Analysis of the flow in layered fluids at small, but finite, amplitude with application to mullion structures (unpublished.)
Fletcher, R. C. & Sherwin, J. 1978. Arc lengths of single layer folds: a discussion of the comparison between theory and observation. *Am. J. Sci.* **278**,1085–1098.
Griggs, D. T., Turner, F. J. & Heard, H. C. 1960. Deformation of rocks at 500 to 800°C. *Mem. geol. Soc. Am.* **79**, 39–104.
Heard, H. C. & Carter, N. L. 1968. Experimentally induced "natural" intragranular flow in quartz and quartzite. *Am. J. Sci.* **266**, 1–42.
Heard, H. C. & Rayleigh, C. B. 1972. Steady-state flow in marble at 500°C to 800°C. *Bull. geol. Soc. Am.* **83**, 935–936.
Hudleston, P. J. 1973. An analysis of "single-layer" folds developed experimentally in viscous media. *Tectonophysics* **16**, 189–214.
Parrish, D. K. 1973. A nonlinear finite element fold model. *Am. J. Sci.* **273**, 318–334.
Parrish, D. K., Krivz, A. L. & Carter, N. L. 1976. Finite-element folds of similar geometry. *Tectonophysics* **32**, 183–207.
Paterson, M. S. & Weiss, L. E. 1966. Experimental deformation and folding in phyllite. *Bull. geol. Soc. Am.* **77**, 343–373.
Paterson, M. S. & Weiss, L. E. 1968. Folding and boudinage of quartz-rich layers in experimentally deformed phyllite. *Bull. geol. Soc. Am.* **79**, 795–812.
Ramberg, H. 1960. Relationships between length of arc and thickness of ptygmatically folded veins. *Am. J. Sci.* **258**, 36–46.
Shimamoto, T. & Hara, I. 1976. Geometry and strain distribution of single-layer folds. *Tectonophysics* **30**, 1–34.
Smith, R. B. 1975. Unified theory of the onset of folding, boudinage, and mullion structure. *Bull. geol. Soc. Am.* **86**, 1601–1609.
Smith, R. B. 1977. Formation of folds, boudinage, and mullions in non-Newtonian materials. *Bull. geol. Soc. Am.* **88**, 312–320.
Smith, R. B. 1979. The folding of a strongly non-Newtonian layer. *Am. J. Sci.* **279**, 272–287.
Tullis, J. A. 1979. High temperature defomation of rocks and minerals. *Rev. Geophys. Space Phys.* **17**, 1137–1154.
White, S. H., Burrows, S. E., Carreras, J., Shaw, N. D. & Humphreys, F. J. 1980. On mylonites in ductile shear zones. *J. Struct. Geol.* **2**, 175–187.
Williams, J. R., Lewis, R. W. & Zeinkiewicz, O. C. 1978. A finite element analysis of the role of initial perturbations in the folding of a single viscous layer. *Tectonophysics* **45**, 187–200.

APPENDIX

The waxes used were obtained at an arts supply store. Since large variations can occur between batches, a sufficient amount of wax was purchased to complete all the experiments. Paraffin wax had a translucent white colour and was slippery to the touch while the microcrystalline wax was dark brown and tacky. Test cylinders were made by pouring melted wax into open-topped cylindrical aluminum moulds. Upon cooling, the paraffin shrank by about 20% thereby producing a deep central depression. More melted paraffin was poured into this depression to eliminate the hollow. Then the top surfaces of the cylinders of both wax types were shaved flat with a knife. The Instron testing machine has a crossed-head which is driven at constant speeds downward toward a rigid platen equipped with a load cell. The load cell's output is amplified and fed to a chart recorder. This system provides an accurate record of force acting through the test specimen vs displacement. A Plexiglas tank set on the load cell platen served as a water bath. Rigid plastic blocks were used as insulating spacers between the wax cylinder and the steel cross-head. Cylinders were smeared with silicone stopcock grease on both ends to reduce friction. Thin, flexible acetate sheets were placed directly on the greased surfaces. These sheets permitted easy removal of the cylinder from the apparatus after deformation was completed. Cylinders were allowed to equilibrate in the apparatus at a set temperature for several hours.

Most cylinders had height-to-diameter ratios of 1. We also ran several with ratios of 2 and 0.25 to check for possible effects of shape on the stress–strain curves. So that the effect of confining pressure could be investigated, other special runs were conducted in an air pressure vessel. To allow any air pockets trapped in the wax a chance to drain, the cylinders were wrapped in air-tight plastic bags fitted with a tube leading out of the pressure vessel to atmospheric pressure. Confining pressures of 1 and 2 bars were used.

To make layered blocks for the folding and boudinage experiments, paraffin was first moulded in the form of a large flat sheet which was shaved down to the proper thickness. Then it was cut by a steel wire into numerous half blocks. Two half blocks were given corresponding sinusoidal edges by using a sharp knife guided by a special guide plates clamped on either side of the block. Microcrystalline layers were prepared by first moulding a thin sheet (0.5–2.0 mm thick) by pouring melted wax onto the surface of hot water. Upon cooling, this was sliced to the proper rectangular shape, heated and softened and then placed between the cool hard paraffin half blocks. These half blocks were then firmly squeezed together to both impart the wavy block edges to the layer and to ensure good adhesion. A square grid pattern was then inked into fine score lines on the front of the block with a permanent ink marking pen.

As in the cylinder tests, the wax blocks were greased and then thin transparent acetate sheets were pressed against the surfaces. The block was placed between rams of the squeeze box and then the Plexiglas view plates were clamped to the front and back by a frame tightened with four thumb screws. The entire squeeze box was then immersed in the water bath and allowed to equilibrate for several hours before the run was conducted.